International Journal of Heat and Mass Transfer 271 (2026) 129335

Contents lists available at ScienceDirect

International Journal of Heat and Mass Transfer

journal homepage: www.elsevier.com/locate/ijhmt

Optimization of tree–like pipelines based on constructal theory for multi–flow regimes

Tian Zhou [a,b], Jinliang Xu [a,b], Xiongjiang Yu [a,b,*], Yan Wang [b], Chao Liu [b], Qinghua Wang [b], Yuguang Niu [a,b], Jizhen Liu [a,b]

[a] State Key Laboratory of Alternate Electrical Power System with Renewable Energy Sources, North China Electric Power University, Beijing 102266, China
[b] Beijing Huairou Laboratory, Huairou District, Beijing 101400, China

ARTICLE INFO

Keywords:
Tree–like pipelines
Murray's law
Multi–flow regimes
Constructal theory
Transitional flow

ABSTRACT

Tree–like pipelines can equalize flow and reduce pressure losses in engineering. Murray's law and its extensions assume the existence of only one flow regime within a structure and derive optimal parameters based on friction coefficient formulas under laminar and turbulent flow. They become invalid in transitional flow and multi–flow regimes (e.g., transitional–laminar coexistence). This study utilizes constructal theory to identify the optimal architecture for multi–flow regimes, with the goal of minimizing pressure drop, addressing this critical gap. Contrary to Murray's law, which yields a fixed diameter ratio of $2^{-1/3}$, results indicate that when the Reynolds number at the parent pipe (Re_0) varies from 100 to 10^7, the optimal diameter ratio ranges between 0.691 and 0.791, while the optimal bifurcation angle fluctuates between 0° and 75°. The results are compiled into an optimization map, which engineers use to determine the parameters under operating conditions by calculating Re_0 to identify the corresponding region in Fig. 9 and using the calculation formulas in Table 2 and Table 3 for that region. The calculation of pressure drops under multi–flow regimes in the tree–like channels showed that the proposed diameter ratio experiences an 8.5% lower pressure drop compared to Murray's law. In subsequent experimental verification of the derived results, the deviation between experimental values and theoretical predictions does not exceed 15%. The study provides a fluid–mechanics–based framework for advancing the engineering design of tree–like pipelines, with direct relevance to applications such as fluid transport and cooling networks.

1. Introduction

Tree–like fractal networks are widespread in nature [1]. The formation of these fractal patterns results from transport systems inherently seeking the most economical and efficient pathways for the transfer of matter and energy [2]. By applying similar principles to engineering, researchers have developed a biomimetic tree–like branching pipe system. This innovative design employs multi–level bifurcation and hierarchical size scaling to achieve uniform flow distribution. Furthermore, by adjusting the diameter ratios between successive branches and optimizing the angles between them, the system minimizes pressure losses during fluid transport. Consequently, owing to its enhanced performance, the biomimetic tree–like branching pipe structure has been widely adopted in fields such as chemical engineering [3,4], fuel cells [5], and microchannel heat sinks [6,7].

To achieve efficient fluid transportation, it is necessary to optimize the geometric parameters of the bionic tree bifurcation pipeline according to the specific engineering environment. A widely adopted optimization theory in engineering design is Murray's law, proposed by British physicist James Murray in 1926. In his study of biological vascular systems, Murray employed several reasonable assumptions–-that the fluid is Newtonian, the flow channel is a straight cylindrical tube, the fluid viscosity is constant, and the flow is laminar. By applying the Hagen–Poiseuille equation, he derived a law stating that when the total energy consumption is minimized, the cube of the radius of the parent vessel equals the sum of the cubes of the radius of the daughter vessels [8]. In addition to vascular fractal systems, numerous other biological fractal systems adhere to Murray's law, particularly in the mammalian respiratory system–for instance, the flow of gases in the lungs and blood in capillaries [9]. Moreover, Murray's law is applicable

* Corresponding author at: State Key Laboratory of Alternate Electrical Power System with Renewable Energy Sources, North China Electric Power University, Beijing 102266, China.
E-mail address: yuxiongjiang@ncepu.edu.cn (X. Yu).

https://doi.org/10.1016/j.ijheatmasstransfer.2026.129335
Received 8 April 2026; Received in revised form 29 June 2026; Accepted 21 July 2026
Available online 28 July 2026
0017-9310/© 2026 Elsevier Ltd. All rights are reserved, including those for text and data mining, AI training, and similar technologies.

to inanimate systems as well [10,11], establishing it as a fundamental and universal principle governing biological fractal transport mechanisms. This principle has also been corroborated through experimental investigations [12,13].

Murray's law defines the optimal proportion of pipe diameters in a tree–like network to minimize pressure drop. However, the law has limitations, particularly in engineering applications involving turbulence, non–Newtonian fluids, or other conditions that violate its underlying assumptions. Consequently, to extend the utility of tree–like pipelines for energy saving and reduced consumption under a broader range of conditions, numerous researchers have undertaken expanded investigations based on Murray's law (Table 1). Barati et al. [14] incorporated the pulsatile pressure gradient generated by the periodic beating of the heart into an extended study of Murray's law. For symmetric bifurcations, the influence of the Womersley number was introduced into the formula for the optimal diameter ratio. The results show that when the Womersley number ranges from 2 to 5, the diameter exponent changes from 3 in Murray's law to approximately 3.2, and the optimal bifurcation angle increases from 75° to about 82°. Garg et al. [15] systematically investigated turbulent flow of power-law fluids in tree–like conduits and derived optimal scaling laws under volume constraints and surface area constraints. The derivation results show that under the condition of smooth walls with a volume constraint, the optimal diameter ratio is $N^{(10n+1)/(24n+3)}$, where N is the number of daughter pipes per parent pipe and n is the power-law index. Under the condition of smooth walls with a surface area constraint, the optimal diameter ratio is $N^{(10n+1)/(21n+2)}$. Under the condition of rough walls with a volume constraint, the optimal diameter ratio is $N^{-3/7}$. Under the condition of rough walls with a surface area constraint, the optimal diameter ratio is $N^{-1/2}$. Jing et al. [16] further extended it to minimize resistance in a tree–like microchannel network with a rectangular cross–section and constant height. This work revealed that the network's structural parameters influence the optimal width ratio and hydraulic diameter ratio, the latter of which doesn't adhere to Murray's law but is instead a function of the microchannel height, total volume, length ratio, and initial pipe length. Miguel [17] derived and computed the optimal pipe diameter ratio and bifurcation angle for bifurcated pipes under various conditions–including Newtonian fluid in laminar flow, smooth and rough pipe turbulent flow, pulsatile flow, and non–Newtonian fluid in laminar flow–by employing constructal theory to optimize flow resistance. Moreover, Jing and Song [18] applied constructal theory under separate volume and surface area constraints to optimize tree–like pipe networks for minimal flow pressure drop. Their results demonstrate that while the optimal diameter ratio under volume constraints aligns with Murray's law, under surface area constraints the sum of the squares of 2.5 times the daughter pipe diameters equals the square of 2.5 times the parent pipe diameter.

Based on the literature reviewed, previous extensions of Murray's law have been developed under the assumption that only one flow regime exists within the tree–like pipelines. However, in reality, the Reynolds number of the working fluid changes as it flows through successive generations of pipelines, potentially resulting in different flow regimes across different levels. Moreover, in addition to laminar and turbulent flow, the fluid in practical tree–like pipelines may also exhibit a transitional flow regime that lies between the two. The characteristics of transitional flow differ significantly from those of either laminar or turbulent flow, making it inappropriate to directly apply optimization conclusions derived from purely laminar or turbulent conditions. Therefore, paying attention to the transitional flow regime in tree–like pipelines facilitates the construction of optimization models under multi–flow regimes and enhances the practical relevance of optimizing such networks. Moreover, in studies of turbulent flow in smooth pipes, previous researchers have employed the Blasius formula to calculate the Fanning friction factor; however, this approach is constrained by its applicable Reynolds number range (3000–10^5). We examine the Fanning friction factor formulas across various Reynolds number ranges (as presented in Table S1) to identify formulations that are applicable to transitional flows and to turbulent flows in smooth pipes over a broader effective Reynolds number range. This paper aims to minimize pressure drop due to frictional losses along the flow path by using constructal theory to determine the optimal diameter ratio and bifurcation angle for different flow regimes while considering scenarios where the fluid in both the parent pipe and daughter pipes has the same or different flow states under smooth wall conditions. The proposed framework in this paper is specifically intended to bridge the gap between existing single–flow regime Murray's law extensions and realistic multi–flow regimes pipeline systems.

The above introduction first outlines the fundamental concept of tree–like pipelines and advantages in practical applications. It then reviews current development in optimization theories applied to such structures and identifies existing research gaps. Finally, it presents the innovations of this paper and the subsequent research content.

2. Construction of computational models

Constructal theory was introduced by Professor Adrian Bejan of Duke University in 1996 during his modeling and mathematical analysis of the formation and evolution of street networks. At its core, constructal theory posits that any finite–size flow system undergoing structural evolution over time–or in response to environmental imperatives for survival–naturally develops configurations that progressively reduce flow resistance. In other words, the structure of systems originates from the pursuit of optimal performance [19]. In line with constructal theory principles, the optimization work in this paper can be viewed as a generative problem aimed at minimizing the global flow pressure drop under a fixed volume constraint. When applying constructal theory to the optimization of a specific problem, the standard procedure involves several key steps: first, clearly defining the subject of optimization, the objectives, the fundamental assumptions, and the constraints that must be maintained; second, formulating the objective function using the appropriate equations; third, integrating the objective function with the constraints by means of the Lagrange multiplier method to construct the complete optimization function; and finally, determining the function's minimum value via partial differentiation.

This paper focuses on optimizing a symmetric, tree–like branched pipeline structure, as illustrated in Fig. 1. The optimization is carried out under the constraint of a constant overall pipeline volume. The primary objective is to minimize the total pressure drop due to frictional losses along the network. The pipeline is oriented horizontally, where d_0 and l_0 denote the diameter and length of the parent pipe, and d_1 and l_1 correspond to the diameter and length of the daughter pipes, respectively. The parameter θ_m refers to the unique angle between the daughter pipes when the diameter ratio between the daughter and parent pipes meets the requirement that satisfies the condition of minimizing the total pressure drop under the two constraints of volume conservation and fixed inlet and outlet endpoints. In engineering applications, most working fluids, such as air and water, are Newtonian. Moreover, the pipelines in fluid transport networks usually have a large

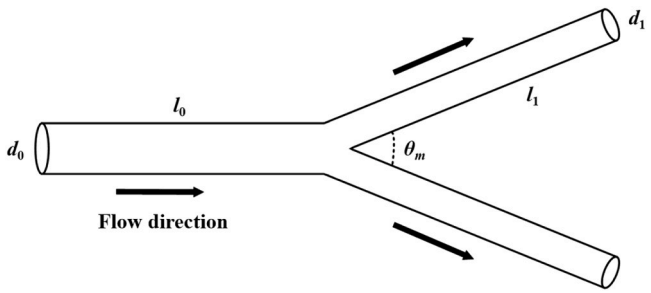


Fig. 1. Symmetrical tree-like branched pipeline structure.

pipeline length; the local loss can be neglected. This paper primarily investigates the transportation process of fluid within pipelines and does not involve the process from the container to the pipe network; therefore, entrance section loss is not considered. The roughness of commonly used stainless steel pipes is relatively low, resulting in friction closely approximating smooth pipes. Therefore, it is assumed that the pipeline features a circular cross–section with smooth walls and that the internal working fluid is Newtonian, flowing under constant temperature conditions and entrance effects and localized resistances at branch junctions are considered negligible. Fig. 2 compares the computed results of various Fanning friction factor formulas applicable to transitional flow regimes within their respective valid ranges [20–27]. Among numerous transition flow formulas, Ghajar et al. [23] accounted for the entrance effect, Li et al. [25] derived for semi-circular pipes, and Wang et al. [27] considered significant roughness. These are inconsistent with the physical model herein and not adopted. Among remaining formulas, Bhatti [20] is simpler and facilitates more efficient subsequent theoretical derivations, although computational results are similar. This formula not only has a simple form and efficient computational performance, but also its accuracy in straight pipes has been extensively validated by experimental data. Tam et al. [28] employed a horizontal straight circular pipe with a right–angle inlet to measure the friction coefficient of an ethylene glycol–water mixture under isothermal conditions in the transitional flow regime, and the deviation between the experimental results and the formula was approximately 10.8%. Sun et al. [29] tested the friction coefficient of deionized water in straight pipes under adiabatic conditions in the transitional flow regime, with a deviation of about 9.4% from the formula. Karwa et al. [30] investigated the pressure drop characteristics of air in smooth rectangular cross–section ducts, and the friction coefficient values obtained in the transitional flow regime deviated from Bhatti's formula by approximately 5.9%. Varnaseri et al. [31] tested the hydraulic performance of polyacrylamide in horizontal smooth circular pipes at different Reynolds numbers, and the data obtained in the transitional flow regime showed a deviation of about 8.9% from the calculated values of the formula. Wang et al. [32] examined the flow characteristics of deionized water in straight pipe sections under adiabatic conditions; the experimental data indicated good agreement between the friction coefficient values and the formula predictions in the transitional flow regime. The experiments reported in these references employed Newtonian fluids such as air, nitrogen, and water, and the test sections used in the experiments were horizontal straight pipes with sufficiently large length–to–diameter ratios. These conditions are highly consistent with the assumptions of the physical model in this study. Moreover, Bhatti's formula [20] demonstrated extremely high accuracy under these experimental scenarios, indicating that this formula is highly applicable to the physical model established in this paper. The specific content of the formula is as follows : .

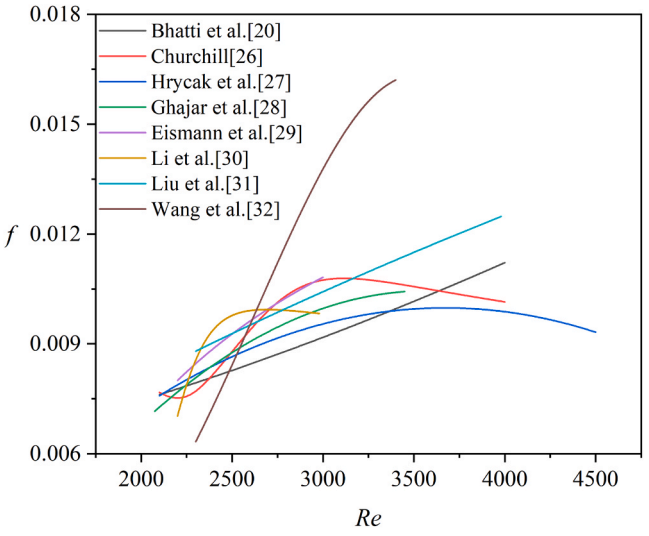


Fig. 2. Comparison of the results from different calculation formulas for the Fanning friction factor in transitional flow.

Fanning friction coefficient formula for the laminar flow region ($Re < 2100$) :

$$f = \frac{16}{\mathrm{Re}} \tag{2 -1}$$

Fanning friction coefficient formula for the transitional flow region ($2100 \le Re \le 4000$) :

$$f = 5.4 \times 10^{-3} + 2.3 \times 10^{-8} Re^{1.5} \tag{2 -2}$$

Fanning friction coefficient formula for the turbulent flow region ($4000 < Re < 10^7$) :

$$f = 1.28 \times 10^{-3} + 0.1143 Re^{-0.311} \tag{2 -3}$$

3. Results and discussion

3.1. Single–phase flow

Assuming that the working fluid exhibits an identical flow regime in both the parent and daughter pipes, separate computational models for laminar, transitional, and turbulent flows are developed based on constructal theory.

3.1.1. Laminar flow

Under the constraint of volume, Bejan used constructal theory to derive that when the working fluid in both the parent and daughter pipes is in a laminar state and the flow pressure drop is minimized, the diameter ratio d_1/d_0 should be $2^{-1/3}$, which is consistent with Murray's law [33]. After obtaining the optimal diameter ratio, Miguel [17] derived the calculation formula for the optimal bifurcation angle θ_m of a tree–like pipeline under the constraint of volume conservation, as shown in Equation (3−1). This formula is applicable to all flow regimes; by substituting the optimal diameter ratio for the laminar regime, the resulting optimal bifurcation angle is approximately 75°, aligning with Murray's findings [34]. In addition, Stephenson et al. [35] observed that the three constraint options (pressure–drop minimization, volume minimization, and flow–rate maximization) all lead to the same optimal daughter–parent area ratio. In other words, the optimal diameter ratio and bifurcation angle derived under laminar flow conditions as well as under subsequent operating scenarios also satisfy the requirements of minimizing pressure drop under volume constraints and minimizing the overall pipeline volume under pressure drop constraints.

$$\cos\theta_m = \frac{1 - 2(d_1/d_0)^4}{2(d_1/d_0)^4} \tag{3 -1}$$

3.1.2. Transitional flow

In the transitional flow regime, the fluid pressure drop is quantified using a formula based on the pressure drop per unit weight of the fluid. Under these conditions, the Reynolds number (Re_0) measured at the inlet of the parent pipe ranges from 2100 to 4000:

$$\Delta P = \lambda \cdot \frac{l}{d} \cdot \frac{\rho v^2}{2} \tag{3 -2}$$

$$\lambda = 4 \times \left(0.0054 + 2.3 \times 10^{-8} Re^{1.5}\right) \tag{3 -3}$$

In the equation above, λ denotes the friction loss coefficient along the pipe, which is equivalent to four times the Fanning friction coefficient, and v represents the flow velocity. Accordingly, the total pressure drop ΔP_t in the pipeline is expressed in terms of the parent pipe's friction coefficient λ_0, flow velocity v_0, and flow rate q_0, as well as the daughter

pipes' friction coefficient λ_1 and flow velocity v_1:

$$\Delta P_t = \lambda_0 \cdot \frac{l_0}{d_0} \cdot \frac{\rho v_0^2}{2} + \lambda_1 \cdot \frac{l_1}{d_1} \cdot \frac{\rho v_1^2}{2} \quad (3\text{-}4)$$

$$\Delta P_t = 4\left(0.0054 + 2.3 \times 10^{-8}\left(\frac{4q_0}{\pi\mu d_0}\right)^{1.5}\right) \cdot \frac{l_0}{d_0} \cdot \frac{8q_0^2}{\pi^2 \rho d_0^4} + 4\left(0.0054 + 2.3 \times 10^{-8}\left(\frac{2q_0}{\pi\mu d_1}\right)^{1.5}\right) \cdot \frac{l_1}{d_1} \cdot \frac{2q_0^2}{\pi^2 \rho d_1^4} \quad (3\text{-}5)$$

According to constructal theory, the expression for the ratio of d_1 to d_0 can be obtained, as shown in Equation (3–6), with the detailed derivation steps provided in Appendix B.

$$\frac{d_1}{d_0} = \sqrt[7]{\frac{0.027 + 1.495 \times 10^{-7} \times Re_0^{1.5}\left(\frac{d_0}{2d_1}\right)^{1.5}}{0.216 + 1.196 \times 10^{-6} Re_0^{1.5}}} \quad (3\text{-}6)$$

Due to the complexity of Equation (3–6), a direct solution is not feasible. To address this, we define $k = d_1/d_0$, which transforms Equation (3–6) into Equation (3–7). By introducing the function $f(k)$ as shown in Equation (3–8), we then seek an approximate solution for $f(k)$ over the interval [0, 1] using the bisection method. The entire procedure was implemented using MATLAB software.

$$\left(0.216 + 1.196 \times 10^{-6} Re_0^{1.5}\right)k^{8.5} - 0.027k^{1.5} - 1.495 \times 10^{-7} \times \left(\frac{Re_0}{2}\right)^{1.5} = 0 \quad (3\text{-}7)$$

$$f(k) = \left(0.216 + 1.196 \times 10^{-6} Re_0^{1.5}\right)k^{8.5} - 0.027k^{1.5} - 1.495 \times 10^{-7} \times \left(\frac{Re_0}{2}\right)^{1.5} \quad (3\text{-}8)$$

Fig. 3 presents the final solution outcomes. As depicted in Fig. 3(a), when the diameter ratio satisfies the condition for minimizing flow pressure drop, the Reynolds number in the daughter pipes (Re_1) increases from 1446 to 2800 as Re_0 increases from 2100 to 4000. When Re_1 equals 2100, Re_0 is approximately 3023.4. Since the calculations assume that the fluids in both the parent and daughter pipes are in a transitional state, the data presented in Fig. 3(b) correspond to Re_0 values of 3023.4 and above. The red line indicates that the optimal diameter ratio (d_1/d_0) decreases almost linearly from 0.719 to 0.7142 as Re_0 increases, with only a slight overall variation. Substituting these d_1/d_0 values into equation (3–1) yields the variation of the optimal bifurcation angle (θ_m), as illustrated by the black line in Fig. 3(b). θ_m exhibits a similar trend, decreasing from 30° to approximately 22.8° with increasing Re_0.

Due to the variety of formulas available to calculate the transitional friction factor, discrepancies arise in their applicable ranges and calculated values. Consequently, this study employs multiple formulas to compute the transitional friction factor and derive d_1/d_0. As illustrated in Fig. 3(c), although the optimal diameter ratios obtained from different formulas vary with changes in Re_0, the numerical differences are minimal. The maximum value in Fig. 3(c) is approximately 0.77, whereas the minimum value is around 0.7, resulting in a deviation of about 10%. Moreover, the formula adopted in this study is more concise, thereby enhancing computational efficiency.

3.1.3. Turbulent flow

In turbulent flow, the pressure drop is expressed using the standard pressure drop formula for a unit weight of fluid. In this regime, Re_0 ranges from 4000 to 10^7, while the friction factor along the length of the pipe is:

$$\lambda = 4 \times \left(1.28 \times 10^{-3} + 0.1143 Re^{-0.311}\right) \quad (3\text{-}9)$$

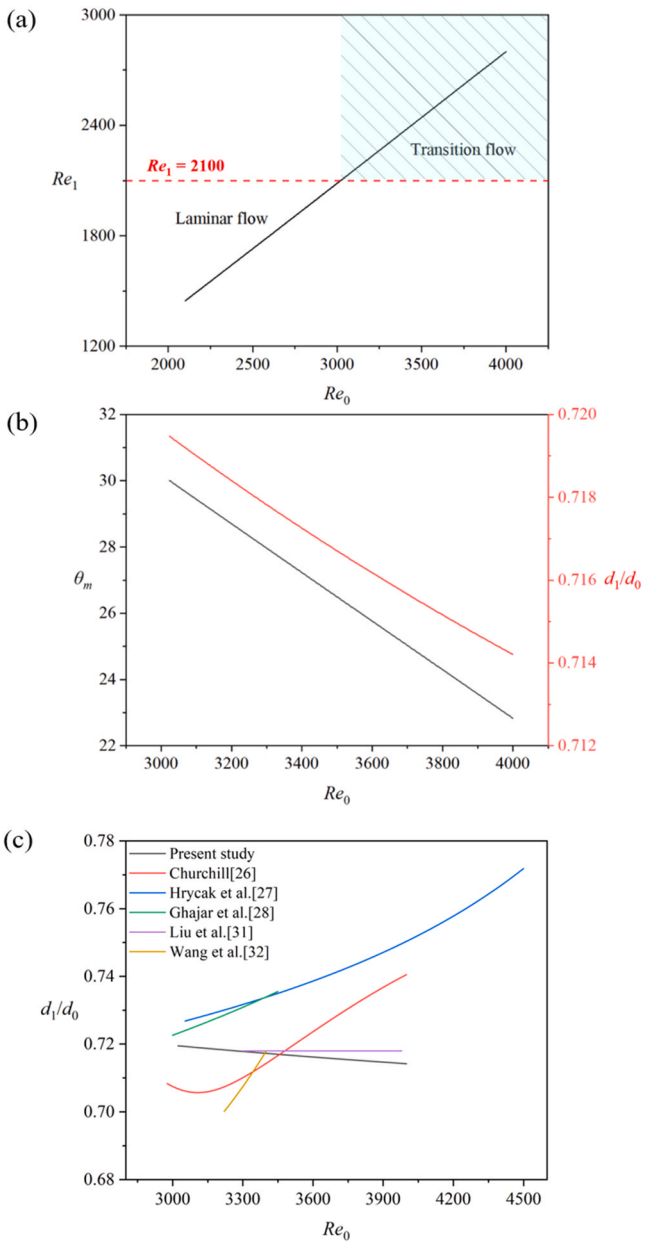


Fig. 3. The influence of initial conditions on the optimal diameter ratio and optimal bifurcation angle in the transitional flow regime. (a) The variation of the Reynolds number Re_1 in the daughter pipes with changes in Re_0; (b) The variation in the optimal diameter ratio (d_1/d_0) and optimal bifurcation angle (θ_m) as Re_0 changes; (c) The variation of d_1/d_0 derived using different transitional flow fanning friction factor formulas as Re_0 changes.

Therefore, the total pressure drop ΔP_t is:

$$\Delta P_t = \frac{8q_0^2}{\pi^2\rho}\left[\left(1.28 \times 10^{-3} + 0.1143\left(\frac{4q_0}{\pi\mu d_0}\right)^{-0.311}\right) \cdot \frac{l_0}{d_0} \cdot \frac{4}{d_0^4} + \left(1.28 \times 10^{-3} + 0.1143\left(\frac{2q_0}{\pi\mu d_1}\right)^{-0.311}\right) \cdot \frac{l_1}{d_1} \cdot \frac{1}{d_1^4}\right] \quad (3\text{-}10)$$

The ratio of d_1 to d_0 can be derived from constructal theory, and the detailed process is presented in Appendix B.

$$\frac{d_1}{d_0}=\sqrt[7]{\frac{6.4\times10^{-3}+0.1143\times4.689Re_0^{-0.311}\left(\frac{d_0}{2d_1}\right)^{-0.311}}{5.12\times10^{-2}+0.9144\times4.689Re_0^{-0.311}}} \quad (3\ -11)$$

Equation (3−11) cannot be solved directly; therefore, a numerical method is employed. The solution process follows the same procedure as that used for the transitional flow regime. Fig. 4(a) illustrates that when Re_0 exceeds 6037, the flow in parent and daughter pipes becomes turbulent. As shown in Fig. 4(b), when both the parent pipe and daughter pipes exhibit turbulent flow (i.e., $Re_0 \geq 6037$), d_1/d_0 depends solely on Re_0. With increasing Re_0, d_1/d_0 gradually decreases from 0.755 to 0.748. Similarly, θ_m decreases from 57.3° to 53.3°, although its reduction is less pronounced than that observed in the transitional regime. In previous studies [17], the Blasius formula was used to calculate the fanning friction factor under turbulent conditions; accordingly, the derived optimal diameter ratio was $2^{-11/27}$ (approximately 0.7539), and substituting this ratio into the formula for the optimal bifurcation angle yielded an angle of about 56.89°. Comparisons between earlier studies and the present work, as depicted in the two curves of Fig. 5, reveal that the discrepancy between the two graphs increases with Reynolds number. This phenomenon is attributed to the decreased accuracy of the Blasius formula when the Reynolds number exceeds its applicable range, leading to deviations in the computed results.

3.2. Coexistence of multiple flow states

After the fluid flows from the parent pipe into the daughter pipes, variations in flow rate and pipe diameter alter the flow velocity, which in turn changes the motion state of the fluid particles, thereby causing a transition in the flow regime. Therefore, theoretically, there should exist multi–flow regimes between the various single–flow regimes discussed earlier. That is, within a specific range of Re_0, the fluid may exhibit different flow regimes in the parent pipe and the daughter pipes. This section examines this phenomenon in detail.

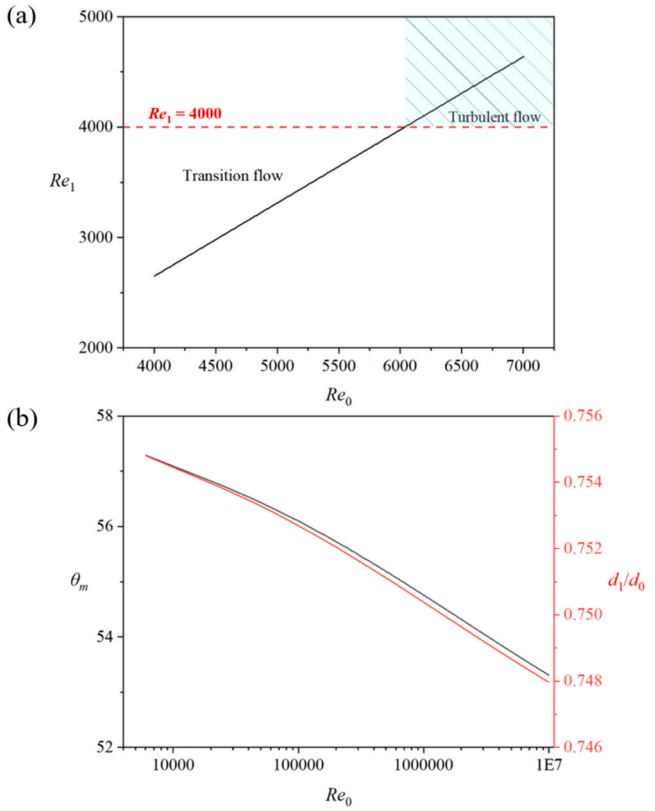


Fig. 4. Variation of Re_1, θ_m, and d_1/d_0 with Re_0 under turbulent flow.

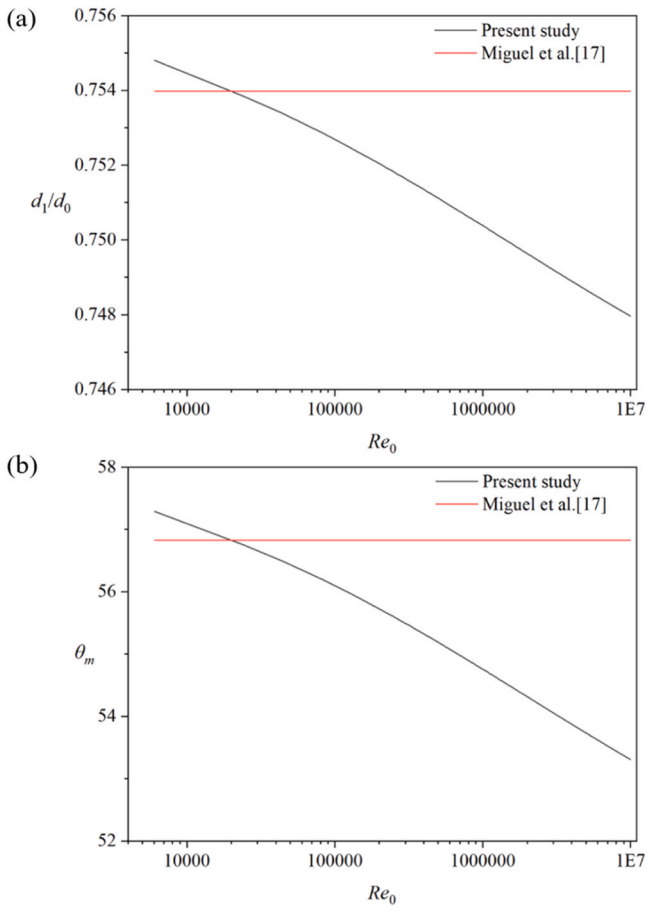


Fig. 5. The comparison of d_1/d_0 and θ_m derived under turbulent flow in present study with those derived in other literature.

3.2.1. Transitional flow in the parent pipe–laminar flow in the daughter pipes

This section discusses the multi–flow regime in tree–liked pipelines occurring between laminar and transitional flow regimes. Assuming the fluid is in transitional flow in the parent pipe, its velocity decreases upon entering the daughter pipes, causing the trajectories of fluid to shift from intermittently chaotic to smooth and orderly. At this point, the fluid within the daughter pipes transitions to laminar flow. The total pressure drop in the pipeline ΔP_t can be formulated as follows:

$$\Delta P_t=\frac{8q_0^2}{\pi^2\rho}\left[\left(0.0054+2.3\times10^{-8}\left(\frac{4q_0}{\pi\mu d_0}\right)^{1.5}\right)\cdot\frac{l_0}{d_0}\cdot\frac{4}{d_0^4}+16\left(\frac{2q_0}{\pi\mu d_1}\right)^{-1}\cdot\frac{l_1}{d_1}\cdot\frac{1}{d_1^4}\right] \quad (3\ -12)$$

Following the previous derivation approach, the ratio of d_1 to d_0 can be obtained as follows, with the detailed derivation steps provided in Appendix B.

$$\frac{d_1}{d_0}=\sqrt[6]{\frac{128}{0.216\mathrm{Re}_0+1.196\times10^{-6}Re_0^{2.5}}} \quad (3\ -13)$$

Fig. 6(a) demonstrates that fluid flow in the daughter pipes remains laminar when Re_0 is less than 2905.5. Consequently, for the fluid to exhibit transitional behavior in the parent pipe while remaining laminar in the daughter pipes, Re_0 should range between 2100 and 2905.5, as illustrated in Fig. 6(b). In this regime, the ratio d_1/d_0 decreases from 0.754 to 0.691 with increasing Re_0, and θ_m declines rapidly; for instance, when Re_0 is 2100, θ_m is approximately 57°, but it approaches 0 as Re_0 increases to 2685.2. Furthermore, Fig. 6(a) indicates that when Re_0

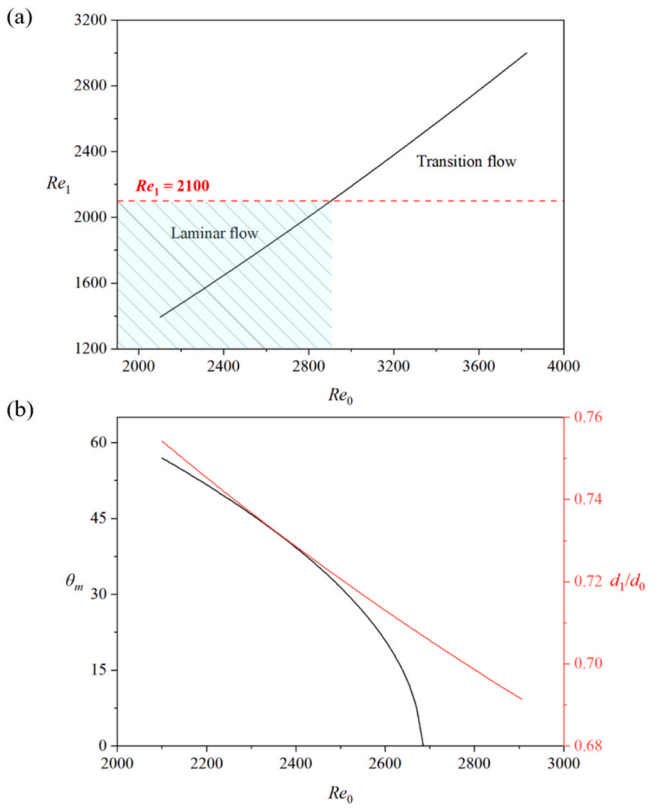


Fig. 6. The variations of Re_1, θ_m, and d_1/d_0 with Re_0 under the condition of transitional flow in the parent pipe and laminar flow in the daughter pipes.

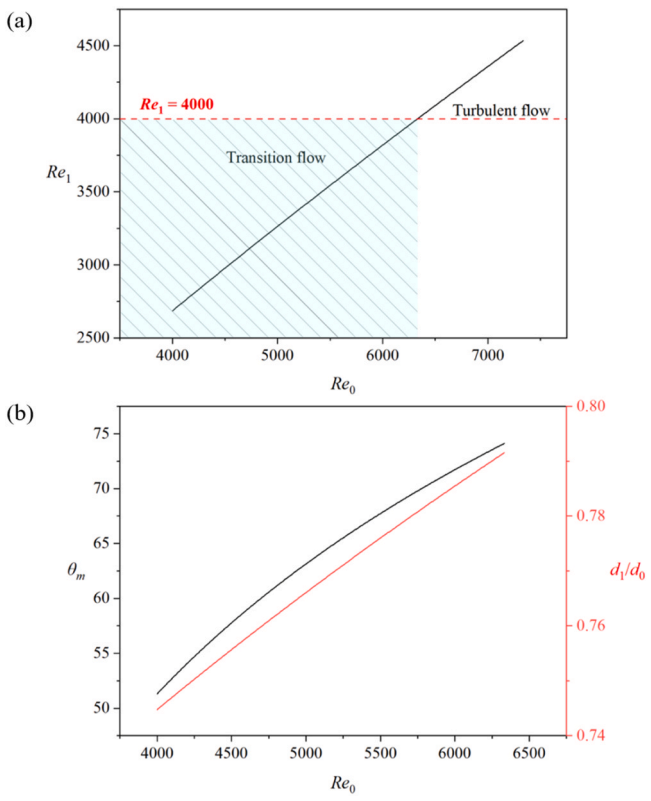


Fig. 7. The variations of Re_1, θ_m, and d_1/d_0 with Re_0 under the condition of turbulent flow in the parent pipe and transitional flow in the daughter pipes.

exceeds 2905.5, the fluid in both the parent and daughter pipes transitions to a turbulent state, whereas Fig. 3(a) identifies this threshold at 3023.4. This discrepancy arises from differing assumptions in the computational models, which lead to variations in the effective parameter ranges.

3.2.2. *Turbulent flow in the parent pipe–transitional flow in the daughter pipes*

In this subsection, the multi–flow regimes exhibited by tree–liked pipelines during the transition between transitional flow and turbulent flow are discussed. Assuming the fluid is in a turbulent state within the parent pipe, its velocity decreases upon entering the daughter pipes, resulting in a reduction of disorder inside the fluid. Although the flow is no longer fully and continuously turbulent, it does not transition into stable laminar flow either. Instead, it exists as an intermittent and unstable transitional flow regime between the two. The total pressure drop ΔP_t in the piping network can be expressed by incorporating the friction factor formulations for both turbulent and transitional flows:

$$\triangle P_t = \frac{8q_0^2}{\pi^2\rho}\left[\left(1.28\times10^{-3}+0.1143\left(\frac{4q_0}{\pi\mu d_0}\right)^{-0.311}\right)\cdot\frac{l_0}{d_0}\cdot\frac{4}{d_0^4} + \left(0.0054+2.3\times10^{-8}\left(\frac{2q_0}{\pi\mu d_1}\right)^{1.5}\right)\cdot\frac{l_1}{d_1}\cdot\frac{1}{d_1^4}\right] \quad (3\text{ -}14)$$

Using constructal theory and incorporating the pressure drop expression, the ratio of d_1 to d_0 can be obtained as follows, with the detailed derivation steps provided in Appendix B.

$$\frac{d_1}{d_0} = \sqrt[7]{\frac{0.027+1.495\times10^{-7}Re_0^{1.5}\left(\frac{d_0}{2d_1}\right)^{1.5}}{5.12\times10^{-2}+0.9144\times4.689Re_0^{-0.311}}} \quad (3\text{ -}15)$$

Fig. 7(a) illustrates that when Re_0 ranges from 4000 to 6330, the working fluid exhibits turbulent flow in the parent pipe and transitional flow in the daughter pipes. Contrary to earlier results, an increase in Re_0 causes d_1/d_0 to rise from 0.745 to 0.791 in Fig. 7(b), with a more pronounced variation than that observed in a single flow regime. Additionally, θ_m increases concomitantly with the diameter ratio, markedly shifting from 51.3° to 74.1°. It is also evident that when Re_0 exceeds 6330, the working fluid in both the parent and daughter pipes displays fully developed turbulent flow, whereas Fig. 5(a) indicates a transition at a Reynolds number of 6037. The discrepancy between these values is attributable to the factors discussed in Section 3.2.1 ().

Table 1
Summary of extended research on Murray's law.

Author	Flow regime	Constraint	Geometric shape	Work fluid
Barati et al. [14]	Pulsating flow	Volume constraint	Symmetrical bifurcated pipeline	Newtonian fluid
Garg et al. [15]	Turbulent flow	Volume constraint / surface area constraint	Symmetrical multi-branch pipeline	Power–law fluid
Jing et al. [16]	Laminar flow	Volume constraint	Symmetrical bifurcated pipeline	Newtonian fluid / non–Newtonian fluid
Miguel [17]	Laminar flow, turbulent flow, pulsating flow	Volume constraint	Symmetrical bifurcated pipeline	Newtonian fluid / non–Newtonian fluid
Jing and Song [18]	Laminar flow	Volume constraint / surface area constraint	Symmetrical bifurcated pipeline	Newtonian fluid

3.2.3. Other types of multi–flow regimes

This study categorizes the flow states of the working fluid into laminar flow, transitional flow, and turbulent flow. From a mathematical perspective, placing two of the three flow states in the parent pipe and the daughter pipes, respectively, yields a total of six combinations. Two of these combinations have already been discussed in Sections 3.2.1 and 3.2.2. In this section, the remaining four combinations are addressed. (1) Case 1: laminar flow in the parent pipe and transitional flow in the daughter pipes, $0 < Re_0 < 2100$, $2100 < Re_1 < 4000$. (2) Case 2: transitional flow in the parent pipe and turbulent flow in the daughter pipes, $2100 < \mathrm{Re0} < 4000$, $\mathrm{Re1} > 4000$. (3) Case 3: laminar flow in the parent pipe and turbulent flow in the daughter pipes, $0 < \mathrm{Re0} < 2100$, $\mathrm{Re1} > 4000$. (4) Case 4: turbulent flow in the parent pipe and laminar flow in the daughter pipes, $Re_0 > 4000$, $0 < Re_1 < 2100$. Using the theoretical derivation approach outlined above, the expressions for the optimal diameter ratio under these four scenarios can be obtained, as shown below:

Case 1:

$$\frac{d_1}{d_0} = \sqrt[7]{\frac{0.027Re_0 + 1.495 \times 10^{-7} \times 2^{-1.5} Re_0^{-0.5} \left(\frac{d_1}{d_0}\right)^{-1.5}}{512}} \quad (3\text{-}16)$$

Case 2:

$$\frac{d_1}{d_0} = \sqrt[7]{\frac{0.0064Re_0^{0.311} + 0.536 \times 2^{0.311} \left(\frac{d_1}{d_0}\right)^{0.311}}{1.196 \times 10^{-6} Re_0^{1.811} + 0.216Re_0^{0.311}}} \quad (3\text{-}17)$$

Case 3:

$$\frac{d_1}{d_0} = \sqrt[7]{\frac{0.0064Re_0 - 0.536 \times 2^{0.311} Re_0^{0.689} \left(\frac{d_1}{d_0}\right)^{0.311}}{512}} \quad (3\text{-}18)$$

Case 4:

$$\frac{d_1}{d_0} = \sqrt[6]{\frac{16}{6.4 \times 10^{-3} Re_0 + 0.536Re_0^{0.689}}} \quad (3\text{-}19)$$

Fig. 8 presents the solution results for the four aforementioned flow regime combinations. It can be observed from the figure that Re_1 for each flow regime does not fall within the range assumed by its respective hypothesis. Therefore, these flow regime combinations will not be considered in the subsequent analysis.

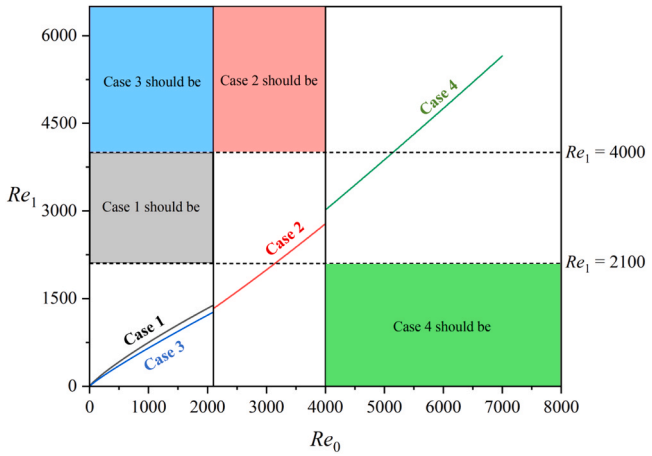


Fig. 8. The values of Re_1 obtained under the four flow regime combinations.

3.3. Summary of calculation results

3.3.1. Description of the optimization map

Fig. 9 provides a comprehensive summary of the computational results. The horizontal axis corresponds to the inlet Reynolds number of the parent pipe (Re_0), while the vertical axis represents the Reynolds number in the daughter pipes (Re_1). The red sections, labelled with Roman numerals, delineate the Reynolds number ranges examined in this study, with detailed information presented in Table 2 and Table 3. Region I indicates that both the parent pipe and the daughter pipes are in laminar flow; Region II indicates that the parent pipe is in transitional flow while the daughter pipes are in laminar flow; Region III indicates that both the parent pipe and the daughter pipes are in transitional flow; Region IV indicates that the parent pipe is in turbulent flow while the daughter pipes are in transitional flow; Region V indicates that both the parent pipe and the daughter pipes are in turbulent flow. The procedure for using the optimization map involves three steps: (1) calculating the Reynolds number of the working fluid at the inlet of the parent pipe based on the system parameters. (2) selecting the corresponding region in Fig. 9 based on the Reynolds number of the parent pipe. (3) finding the formulas for the optimal diameter ratio and bifurcation angle in the corresponding region from Table 2 and Table 3, then substituting the Reynolds number into these formulas for calculation. For the discontinuity between Region II and Region III, a linear interpolation method is employed to connect the optimal parameters at the boundaries of the two regions, thereby obtaining the optimal parameter distribution in that section. For the overlapping region between Region IV and Region V, it indicates that within the overlapping range of Reynolds numbers, the flow regime in the tree–like pipelines can be either transitional flow or a combination of turbulent and transitional flow. In both cases, there exist corresponding optimal diameters and optimal bifurcation angles. The specific choice of flow regime depends on the particular requirements of the application.

The optimization diagram encompasses all possible single–flow and multi–flow regimes combinations within a single bifurcating tree–like pipeline and provides the corresponding Reynolds number ranges in the parent and daughter pipes under each scenario, as well as the optimal diameter ratio and optimal bifurcation angle. The integration of multi–flow regimes serves as a critical nexus in constructing the optimization map. Considering multi–flow regimes bridges the gaps between conclusions drawn from individual single–flow regimes and provides a clearer depiction of the evolution of flow patterns within the entire structure as the Reynolds number at the parent pipe inlet increases. This map enriches existing optimization theory, enabling tree–like pipelines

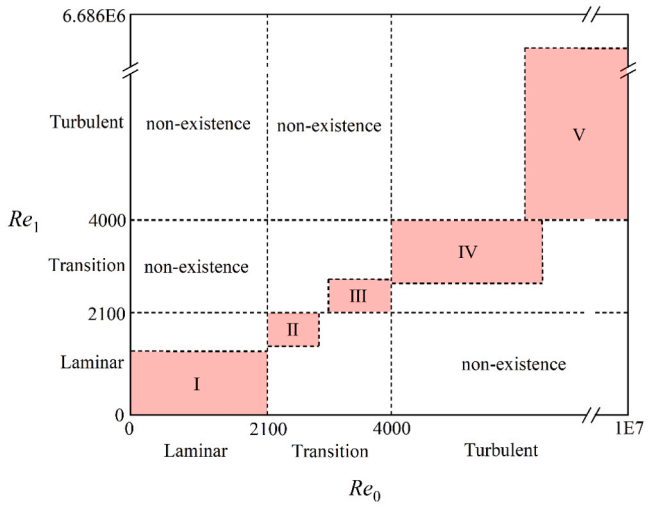


Fig. 9. Optimal graph for symmetrical tree-like pipelines for multiple flow regimes.

Table 2
The optimal diameter ratio among different regions in the optimization map.

Number	The expression of d_1/d_0	The range of d_1/d_0
I	\\	0.794
II	$\frac{d_1}{d_0} = \sqrt[6]{\frac{128}{0.216Re_0 + 1.196 \times 10^{-6}Re_0^{2.5}}}$	0.754–0.691
III	$\frac{d_1}{d_0} = \sqrt[7]{\frac{0.027 + 1.495 \times 10^{-7} \times Re_0^{1.5}\left(\frac{d_0}{2d_1}\right)^{1.5}}{0.216 + 1.196 \times 10^{-6}Re_0^{1.5}}}$	0.719–0.714
IV	$\frac{d_1}{d_0} = \sqrt[7]{\frac{0.027 + 1.495 \times 10^{-7}Re_0^{1.5}\left(\frac{d_0}{2d_1}\right)^{1.5}}{5.12 \times 10^{-2} + 0.9144 \times 4.689Re_0^{-0.311}}}$	0.745–0.791
V	$\frac{d_1}{d_0} = \sqrt[7]{\frac{6.4 \times 10^{-3} + 0.1143 \times 4.689Re_0^{-0.311}\left(\frac{d_0}{2d_1}\right)^{-0.311}}{5.12 \times 10^{-2} + 0.9144 \times 4.689Re_0^{-0.311}}}$	0.755–0.748

Table 3
The optimal bifurcation angle among different regions in the optimization map.

Number	The expression of θ_m	The range of θ_m
I	$\theta_m = \arccos\frac{1 - 2(d_1/d_0)^4}{2(d_1/d_0)^4}$	75°
II		57° to 0°
III		30° to 22.8°
IV		51.3° to 74.1°
V		57.3° to 53.3°

to minimize flow pressure drop under a wider range of conditions, and represents the most important core conclusion of this paper.

3.3.2. Explanation of the physical mechanism

The existence of the optimal diameter ratio essentially reflects the rational allocation of limited volume resources between the parent pipe and daughter pipes under a volume constraint, aiming to minimize the pressure drop. An increase in the parent pipe's diameter is accompanied by a decrease in the daughter pipes' diameters. Enlarging pipe diameters reduces pressure drops, while reducing them increases pressure drops. The optimal diameter ratio precisely represents the equilibrium between these two opposing effects. Analysis of the preceding calculation formulas for pressure drop under different flow regimes reveals that, when flow rate is independent of diameter, the pressure drop in laminar flow is proportional to d^{-4}, in transitional flow it is approximately proportional to $d^{-6.5}$, and in turbulent flow it is approximately proportional to $d^{-4.689}$. This indicates that the pressure drop is most sensitive to diameter in the transitional flow regime and least sensitive in the laminar flow regime.

As Re_0 increases from 2100, the tree–like pipelines first enter Region II, where the parent pipe is in transitional flow while the daughter pipes remain in laminar flow. Since the pressure drop in transitional flow is more sensitive to diameter, increasing the diameter of the parent pipe yields a greater reduction in pressure drop. Therefore, more volume resources should be allocated to the parent pipe to increase its diameter compared to the laminar case, resulting in a decrease in the optimal diameter ratio. As Re_0 further increases, the advantage of sensitivity becomes more pronounced, causing the optimal diameter ratio to continue decreasing with increasing Re_0. When Re_0 increases further into Region III, both the parent and daughter pipes are in transitional flow, and the sensitivity of pressure drop to diameter is the same in both. In this case, the benefit of increasing the parent pipe diameter is relatively reduced, so part of the volume is transferred from the parent pipe to the daughter pipes, leading to a recovery of the optimal diameter ratio. Since the pressure drop in transitional flow is not exactly proportional to $d^{-6.5}$, slight fluctuations occur as Re_0 increases. As Re_0 continues to rise into Region IV, the parent pipe enters turbulent flow while the daughter pipes remain in transitional flow. At this stage, the situation is reversed: the pressure drop in the daughter pipes is more sensitive to diameter, so increasing the diameter of the daughter pipes provides a greater benefit in reducing pressure drop. As a result, the optimal diameter ratio increases significantly compared to Region III. Finally, when entering Region V, where both the parent and daughter pipes are in turbulent flow, the benefit of increasing the diameter of the daughter pipes diminishes, and the optimal diameter ratio decreases compared to Region IV.

The preceding model assumptions do not consider local resistance generated at pipe bifurcations and the impact of bifurcations on the flow process. The optimal bifurcation angle in this paper was obtained by substituting the optimal diameter ratio into Equation (3−1) after determining that ratio. The calculated angle value is a purely geometric necessity–the only geometric solution under the constraints of fixed volume, fixed endpoint positions, and an invariant diameter relationship between the parent and daughter pipes. As such, it offers no room for free adjustment. Therefore, numerically, it follows the same trend as the optimal diameter ratio and does not possess any special physical significance on its own (this conclusion is limited to the assumptions adopted in the present model where local resistance effects are neglected).

3.4. Internal consistency of computational results

To better present derivation results under transitional flow regimes, this study assumes a specific application scenario. As depicted in Fig. 10, a rectangular radiator is analysed, featuring an internal channel with a symmetric tree–like bifurcation structure; each branch diverges at an angle of 60°, and the channel cross–section is circular. The overall dimensions are listed in Table 4, and the internal cooling medium is deionized water at 20°C. The following assumptions were made for the calculations: (1) The channel interiors are horizontal and smooth, the fluid is fully developed prior to entering the radiator channels, and local losses at the bifurcations are neglected; (2) The analysis focuses solely on the pressure drop of the fluid, and fluid property variations are temporarily ignored, with the density assumed to be 1000 kg/m^3 and the dynamic viscosity 1.002×10^{-3} Pa·s. To ensure that the fluid enters the channels under the combined flow regime of transitional flow and laminar flow, the inlet mass flow rate is maintained within the range of 6.1×10^{-3} kg/s to 7.2×10^{-3} kg/s. Furthermore, to emphasize the optimization effect, an optimization group is established alongside control groups A and B. The structures of the optimization group, control group A, and control group B are all shown in Fig. 10, with the only difference being the selected diameter ratios. The optimization group selects diameter ratios at each level based on the transitional flow derivation results presented in this paper (≈ 0.72), whereas control group A employs the $2^{-1/3}$ (≈ 0.794) ratio as recommended by Murray's law, and control group B determines the diameter ratios to maintain consistent working fluid velocities across all levels (≈ 0.707). Both groups are designed to have an identical total channel volume. The computational results, presented in Fig. 11, demonstrate that the optimization group exhibits a significantly lower pressure drop than the control groups, with the difference becoming more pronounced as the mass flow rate increases. When the flow rate reaches its maximum, the pressure drop in the optimization group is 1718.1 Pa, while that in control group A, based on Murray's law, is 1864.2 Pa. The pressure drop in the optimization group is approximately 8.5% lower than that in control group A. The significant reduction in pressure drop observed in the optimized group not only intuitively demonstrates the inherent limitations of Murray's law under conditions beyond laminar flow but also confirms the internal consistency of the theoretical derivations presented in this paper under multi–flow regimes. In large–scale fluid distribution systems, reducing flow pressure drop can decrease annual pumping energy consumption and yield carbon reduction benefits. For cooling network applications, reducing the flow pressure drop of the

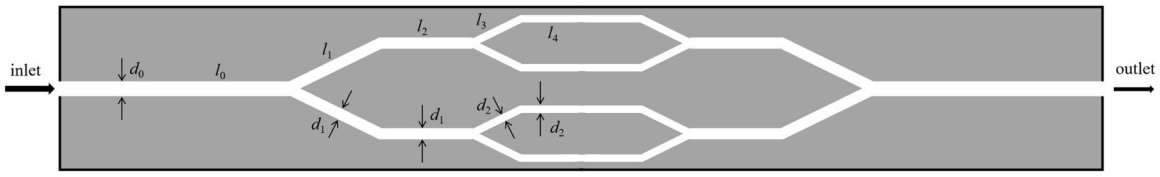


Fig. 10. Schematic diagram of the rectangular radiator.

Table 4
Structural parameters of the rectangular radiator. (unit: mm).

Case	d_0	d_1	d_2	l_0	l_1	l_2	l_3	l_4
Optimized group	2.5	1.775	1.278	18.955	6.634	6.634	4.644	9.288
Control group A	2.283	1.984	1.409	18.955	6.634	6.634	4.644	9.288
Control group B	2.516	1.768	1.255	18.955	6.634	6.634	4.644	9.288

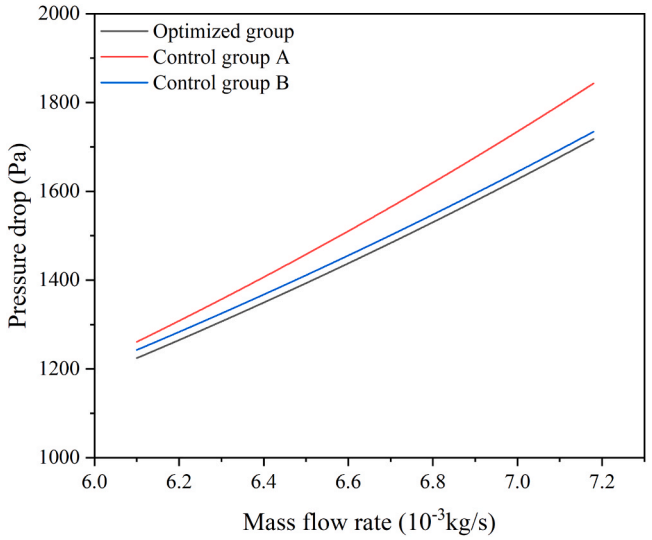


Fig. 11. Comparison of the results between the optimized group and the control groups.

internal cooling medium not only lowers the electricity consumption of the system itself but also improves its energy efficiency metrics.

3.5. Experimental verification

The consideration of multi–flow regimes is the fundamental distinction between this study and other extensions of Murray's law. To better validate the derivation results of this paper under multi–flow regimes, this section designs experiments for verification.

3.5.1. Experimental equipment and procedures

Fig. 12 shows the experimental setup, consisting of a water tank (0.65 m × 0.55 m × 0.65 m), an iron support frame (height: 0.06 m), silicone rubber hoses, a ball valve, a beaker, and a tree–like pipeline component. A small hole is drilled at the bottom of the water tank, connected externally to a silicone hose, which is then linked to the ball valve. The inlet of the tree–like pipeline component is connected to the outlet of the ball valve, while a large–capacity beaker is placed at the outlet to collect water discharged during the test. The tree–like pipeline component comprises two identical symmetric tree–like pipelines, with the outlets of their daughter pipes connected by short silicone hoses. Both the daughter pipes and the parent pipe are made of 316 L stainless steel and are connected via symmetric Y–shaped three–way connectors (304 stainless steel, with an included angle of 30°). In this chapter, four groups of components with different diameter ratios are tested. These four groups have identical internal flow volumes, corresponding to the volume constraint in the previous theoretical derivation. The specific parameters of each component are presented in Table 5. The experimental procedure is as follows: first, the valve is closed, and water is added to the tank. Filling stops when the actual water level is 0.02 m above the designed water level (0.331 m). The valve is then fully opened. Once the water level drops to the designed level, the beaker is placed at the outlet of the component. This measure ensures that the overall flow process has stabilized before measurement begins. Water is collected for 30 s, after which the total volume of outflow is measured. Finally, the corresponding volumetric flow rate q_v is calculated. Each component is tested four times, and the average value is taken.

The design logic of this experiment is to maintain an approximately constant pressure difference across the inlet and outlet of the pipeline components (i.e., the water tank level) during measurement. The flow resistance of water in the components is assessed by the volumetric flow rate at the outlet: a greater volumetric flow rate indicates lower flow resistance. To minimize undeveloped flow section impact on experimental results and considering limitations of the experimental site, this chapter selects Region IV (parent pipe turbulent flow–daughter pipes transitional flow) for validation, which has a larger Reynolds number and a shorter undeveloped section. Based on previous derivation results, the range of Re_0 in Region IV is from 4000 to 6330. Taking $Re_0 = 5000$, the total pressure drop is calculated using Eqs. (3–23) ($\rho_{water} = 1000$ kg/m^3, $\nu_{water} = 1.002 \times 10^{-6}$ m^2/s). The pipe length and diameter in the equation correspond to the parameters of Group Two. After converting the total pressure drop into the corresponding hydraulic head, the value is approximately 0.391 m. Since the height of the support frame is 0.06 m, the designed water level is set at 0.331 m.

3.5.2. Data processing

This study employed measuring cylinders of 500 mL and 250 mL to measure the volume of water flowing into a beaker within a specified testing period. The volumetric flow rate q_v (10^{-6} m^3/s) was calculated using Equation (3−20), where $t = 30$ s, V_1 is the measurement value from the 500 mL cylinder, and V_2 is the measurement value from the 250 mL cylinder. Error analysis was conducted using the Gaussian error propagation formula, as shown in Eqs. (3–21). It was assumed that errors are uniformly distributed within the allowable interval, where u_c represents the standard uncertainty of the result, $u(x_i)$ denotes the uncertainty of the measured quantity, n is the number of measured quantities required to obtain the result, x_i is the measured quantity, f is the expression used to convert the measured quantities into the result, $a(x_i)$ is the permissible error value of the measuring instrument corresponding to the measured quantity, U is the expanded uncertainty, and k is typically taken as 2, corresponding to a confidence interval of approximately 95%. By substituting Equation (3−20), the standard uncertainty of the volumetric flow rate was obtained, as shown in Eqs. (3–22).

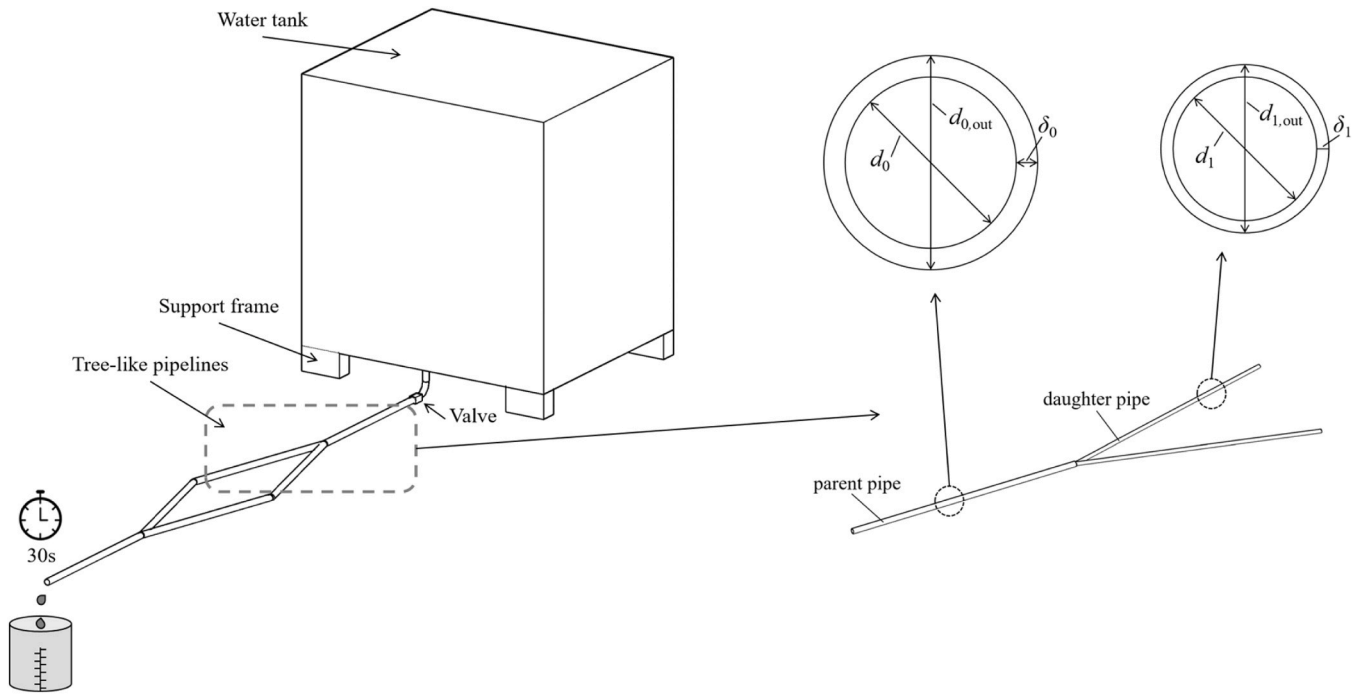


Fig. 12. The structural diagram of the experimental setup (schematic diagram on the left, the cross–sectional view of the pipe for the tree–like pipeline component on the right).

Table 5
Detailed parameters of the tree-like pipeline component. (unit: mm).

Case	d_1/d_0	Parent pipe parameters			Daughter pipe parameters		
		$d_{0,\ out}$	δ_0	Pipe length	$d_{1,\ out}$	δ_1	Pipe length
Group One	0.64	8	0.8	400	4.5	0.2	400
Group Two	0.74	8	1	400	5	0.3	400
Group Three	0.84	7	0.7	400	5.5	0.4	400
Group Four	0.94	7	0.9	400	5.5	0.3	400

According to GB/T 12804–2011, $a(V_1)$ and $a(V_2)$ are 2.5 mL and 1 mL, respectively. Since the test duration was measured manually, and considering the reaction error associated with manual start and stop actions, it was set to 0.2 s

$$q_v = \frac{V_1 + V_2}{t} \tag{3-20}$$

$$u_c = \sqrt{\sum_{i=1}^{n}\left(\frac{\delta f}{\delta x_i}\right)^2 u^2(x_i)} \tag{3-21}$$

$$u(x_i) = \frac{a(x_i)}{\sqrt{3}}$$

$$U = k \cdot u_c$$

$$u_c = \sqrt{\left(\frac{1}{t}\right)^2 u^2(V_1) + \left(\frac{1}{t}\right)^2 u^2(V_2) + \left(\frac{V_1 + V_2}{t^2}\right)^2 u^2(t)} \tag{3-22}$$

3.5.3. Experimental results

Under the designed water level, the change in water tank level before and after the test is approximately 2 mm, accounting for about 0.5% of the hydraulic head. Therefore, the pressure difference across the component inlet and outlet can be considered nearly constant. The test results for each tree–like pipeline component are shown in Fig. 13. The

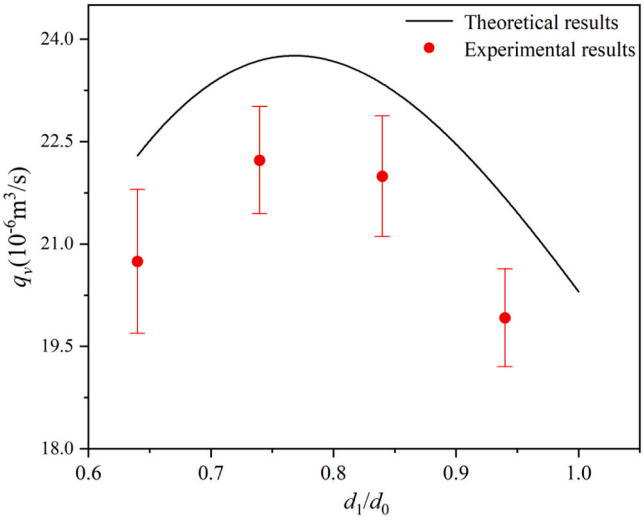


Fig. 13. Comparison of experimental results with theoretically calculated values.

black curves in the figure represent the theoretical volumetric flow rates of tree–like pipeline components with different diameter ratios, solved inversely using Eqs. (3–23) under the same volume constraint and known total pressure drop. The red dots indicate the average values of four volumetric flow rate measurements for each component, while the red lines above and below the dots represent the maximum and minimum values among the four measurements, respectively. It can be observed that the experimental averages follow the same trend as the theoretical values. The diameter ratio of Group Two is closest to the optimal diameter ratio, resulting in the largest average volumetric flow rate. The deviation between the experimental average and the corresponding theoretical value for each group did not exceed 15%, indicating good accuracy. The expanded uncertainty U of the experimental average values across all groups ranges from $0.28 \times 10^{-6}m^3/s$ to

$0.32 \times 10^{-6}m^3/s$. The calculated measurement uncertainty provides a confidence interval within which the true experimental value is likely to fall, thereby making the expression of the measurement results more complete. During the experiment, after the water flows out of the tank, it first passes through a 90–degree elbow and a fully open valve before entering the component. Within the component, the water undergoes splitting and merging processes at the symmetrical Y–type tee junctions and flows through the short–curved sections at the outlet connections of the daughter pipes. These processes introduce additional local losses and disturbances that were not considered in the theoretical calculations, causing the actual flow resistance to be greater than the theoretical case. As a result, the experimentally measured volumetric flow rate is lower than the theoretically calculated value. The good agreement between the experimental results and theoretical calculations not only demonstrates the accuracy of the theoretical model proposed in this study but also confirms the applicability of the derived results under multi–flow regimes.

3.6. Limitations and future directions

This chapter describes the research's relevance to practical applications, its limitations, and directions for future research. The physical model's assumptions in this paper include smooth walls, Newtonian fluids, symmetric bifurcations, neglected property variations, and disregarded inlet effects and local resistance. These assumptions are based on the characteristics of commonly used working fluids in existing engineering applications (such as water, air, and natural gas–Newtonian fluids) and the typical features of pipes in fluid transport industries (low roughness and large pipeline length). However, such model assumptions may still exhibit significant limitations in certain scenarios: (1) When the working fluid is transported through cast pipes or other pipes with high roughness, the friction coefficient formula for smooth pipes cannot calculate the internal pressure drop accurately. (2) For short transport sections, the local resistance and inlet effects of the pipes cannot be neglected. (3) Some working fluids, such as polyethylene, jams, and slurries, exhibit non–Newtonian behavior during flow and require specific non–Newtonian fluid formulas for calculation. (4) In scenarios involving heating or cooling, the physical properties of the working fluid within the pipe change significantly; applying the assumption of constant properties can lead to substantial deviations. (5) In certain cases, due to spatial layout characteristics, the tree–like pipe network may need to be designed asymmetrically.

Building on the existing foundation, subsequent expansions of optimization theory can incorporate considerations such as surface roughness, local resistance and entrance effects, non–Newtonian fluid formulations, and the coupling of thermal boundary conditions and temperature-dependent working fluid properties. When investigating asymmetric tree–shaped pipe structures, the differing diameters of the parent and daughter pipes may lead to a greater variety of flow regime combinations within the three conduits, necessitating the consideration of more operational scenarios. Furthermore, while minimizing pressure drop remains a primary optimization objective, the inclusion of heat transfer performance as an additional criterion can be explored. In terms of experimental validation, the experimental design in this study is relatively simple and only validates the derived results for a single multi–flow regimes region. Future work could involve further experimental validation and investigation of other multi-flow regimes. Additionally, more complex experimental setups could be constructed, incorporating instruments such as flow meters and pressure gauges to accurately measure pressure loss and flow rate at various stages of the pipelines. This would enable a detailed capture of fluid flow characteristics within the tree–like pipeline, reflecting optimization effectiveness. The aforementioned improvement strategies can render tree–like pipe network optimization more comprehensive, thereby enhancing performance across different application scenarios.

4. Conclusion

This paper proposes an optimization design for symmetrical bifurcated tree–like pipe networks. By minimizing pressure drop, optimal diameter ratio and bifurcation angle are derived under conditions where flow regimes in parent and daughter pipes are either identical or different. Based on these derivations, the optimization map is constructed. This research thus makes a significant contribution toward the realization of high–efficiency energy transmission and effective system integration. The key findings are summarized as follows:

Under the condition of laminar flow in both the parent and daughter pipes ($Re_0 < 2100$), as Re_0 increases, the flow regime within the structure transitions to Region II (parent pipe transitional flow–daughter pipes laminar flow). In this region, the pressure drop in the parent pipe is more sensitive to its diameter, and increasing the parent pipe diameter yields greater pressure drop reduction benefits. Consequently, both d_1/d_0 and θ_m decrease with increasing Re_0. When Re_0 further increases into Region III (parent pipe transitional flow–daughter pipes transitional flow), the pressure drop sensitivity to diameter becomes similar in both pipes, and the benefit of enlarging the parent pipe diminishes relatively. As a result, the values of d_1/d_0 and θ_m increase compared to Region II. With continued Re_0 increases to Region IV (parent pipe turbulent flow–daughter pipes transitional flow), the pressure drop in the daughter pipes becomes more sensitive to diameter than the parent pipe, making the daughter pipes enlargement more advantageous. Thus, both d_1/d_0 and θ_m increase with Re_0. Finally, entering Region V (parent pipe turbulent flow–daughter pipes turbulent flow) results in no longer prominent advantages of enlarging the daughter pipes, and both d_1/d_0 and θ_m decrease compared to Region IV.

This study examines a rectangular radiator featuring an internally distributed, tree–like cooling network. Under conditions where transitional and laminar flows coexist, the results derived were compared with Murray's law and the arrangement method where the total cross–sectional area of pipes at all levels remains constant. The calculation results effectively demonstrate the superiority of the proposed multi–flow regimes optimization method over other methods in terms of flow drag reduction. This paper also experimentally validated the derived results under conditions where turbulence and transitional flow coexist. The experimental data indicate a good agreement between the experimental values and the theoretical values, with a deviation of no more than 15%. This finding not only demonstrates the accuracy of the theoretical model proposed in this paper but also confirms the practical applicability of the derived results under multi–flow regimes.

CRediT authorship contribution statement

Jinliang Xu: Supervision, Methodology, Funding acquisition. **Tian Zhou:** Writing – review & editing, Writing – original draft, Investigation, Formal analysis. **Yan Wang:** Supervision, Methodology, Formal analysis. **Xiongjiang Yu:** Supervision, Methodology, Formal analysis. **Qinghua Wang:** Supervision, Project administration, Funding acquisition. **Chao Liu:** Methodology, Formal analysis. **Jizhen Liu:** Methodology. **Yuguang Niu:** Supervision, Methodology.

Declaration of Competing Interest

We state that the manuscript titled as " **Optimization of Tree—Like Pipelines Based on Constructal Theory for Multi—Flow Regimes** " by Tian Zhou, Jinliang Xu, Xiongjiang Yu, Yan Wang, Chao Liu, Qinghua Wang, Yuguang Niu, Jizhen Liu does not have any conflict of interest including any financial, personal or other relationships with other people or organizations.

Acknowledgments

This research is supported by the Coal-Major Project

(2024ZD1700300).

Appendix A. Supporting information

Supplementary data associated with this article can be found in the online version at doi:10.1016/j.ijheatmasstransfer.2026.129335.

References

[1] G.B. West, J.H. Brown, B.J. Enquist, A general model for the origin of allometric scaling laws in biology, Science 276 (5309) (1997) 122–126.
[2] M. Buchanan, Prediction: a game of chance, Nature 419 (6909) (2002) 787, 787.
[3] B. Zhu, Z. Zhang, J. Shi, W. Zheng, Q. Liu, H. Wang, T. Zhang, Q. Yang, J. Zhang, Q. Zhao, Mass transfer control mechanism of CO_2 absorption in MEA-EG solution within the tree-shaped parallel microchannel based on Murray's law, Sep. Purif. Technol. (2025) 134206.
[4] W. Han, W. Li, H. Zhang, Insight into mixing performance of bionic fractal baffle micromixers based on Murray's Law, Int. Commun. Heat. Mass. Transf. 157 (2024) 107843.
[5] J. Choi, Y. Park, J. Park, C. Kim, S. Heo, S.-D. Kim, H. Ju, Innovative flow field design strategies for performance optimization in polymer electrolyte membrane fuel cells, Appl. Energy 377 (2025) 124551.
[6] G. Wang, K. Sheng, Y. Wang, G. Ding, D. Xie, Thermal hydraulic performance of tree-like microchannel heat sink with high branching level based on the improved Murray's law, Int. J. Heat. Mass. Transf. 231 (2024) 125875.
[7] J. Wang, S. Tang, Z. Song, X. Fan, C. Gao, A novel three-dimensional topology-optimized cold plate design for lithium-ion battery thermal management based on Murray's law, Int. J. Heat. Fluid. Flow. 116 (2025) 109997.
[8] C.D. Murray, The physiological principle of minimum work: I. The vascular system and the cost of blood volume, Proc. Natl. Acad. Sci. 12 (1926) 207–214.
[9] A.G. Roy, M.J. Woldenberg, A generalization of the optimal models of arterial branching, Bull. Math. Biol. 44 (1982) 349–360.
[10] E. Azpeitia, G. Tichtinsky, M. Le Masson, A. Serrano-Mislata, J. Lucas, V. Gregis, C. Gimenez, N. Prunet, E. Farcot, M.M. Kater, Cauliflower fractal forms arise from perturbations of floral gene networks, Science 373 (2021) 192–197.
[11] C. Eloy, M. Fournier, A. Lacointe, B. Moulia, Wind loads and competition for light sculpt trees into self-similar structures, Nat. Commun. 8 (2017) 1014.
[12] P. Qi, D. Jing, Experimental and numerical study on the hydrothermal performances of a mirror Y-shaped convergent mini-channel heat sink, Case Stud. Therm. Eng. 53 (2024) 103966.
[13] M.A. Khan, M. Suhaib, M.A. Ansari, Investigations on fluid flow and mixing in fractal tree like biomimetic microchannel based on Murray's law, Chem. Eng. Process. -Process. Intensif. 194 (2023) 109564.
[14] P. Barati, M. Saghafian, Optimum geometric bifurcation under pulsating flow assuming minimum energy consumption in cardiovascular system, an extension on murray's law, J. Appl. Fluid. Mech. 15 (2022) 687–695.
[15] A. Garg, H. Mishra, J. Sarkar, et al., Scaling laws for optimal turbulent flow in tree-like networks with smooth and rough tubes and power-law fluids[J], Eur. Phys. J. 140 (2) (2025) 1–20.
[16] D. Jing, S. Song, L. He, Reexamination of Murray's law for tree-like rectangular microchannel network with constant channel height, Int. J. Heat. Mass. Transf. 128 (2019) 1344–1350.
[17] A.F. Miguel, Constructal branching design for fluid flow and heat transfer, Int. J. Heat. Mass. Transf. 122 (2018) 204–211.
[18] D. Jing, J. Song, Comparison on the hydraulic and thermal performances of two tree-like channel networks with different size constraints, Int. J. Heat. Mass. Transf. 130 (2019) 1070–1074.
[19] A. Bejan, Street network theory of organization in nature, J. Adv. Transp. 30 (2) (1996) 85–107.
[20] S. Kakaç, R.K. Shah, W. Aung, Handbook of Single-phase Convective Heat Transfer, 1987.
[21] S.W. Churchill, Comprehensive correlating equations for heat, mass and momentum transfer in fully developed flow in smooth tubes, Ind. Eng. Chem. Fundam. 16 (1) (1977) 109–116.
[22] P. Hrycak, R. Andrushkiw, Calculation of critical Reynolds numbers in round pipes and infinite channels and heat transfer in transition regions, Int. Heat. Transf. Conf. Digit. Libr. Begel. House Inc. (1974).
[23] A.J. Ghajar, K.F. Madon, Pressure drop measurements in the transition region for a circular tube with three different inlet configurations, Exp. Therm. Fluid. Sci. 5 (1) (1992) 129–135.
[24] R. Eismann, R. Adams, An explicit and continuous friction factor correlation for helical tubes with arbitrary roughness, (2018).
[25] J. Li, Y. Li, T. Xiayu, X. Li, R. Zheng, Experimental investigation on transitional flow of supercritical hydrocarbon fuel within straight channels of Printed Circuit Heat Exchangers for hypersonic thermal management systems, Appl. Therm. Eng. 259 (2025) 124905.
[26] S.-h Liu, Y.-p Huang, J.-f Wang, R.-l Liu, Experimental study on transitional flow in straight channels of printed circuit heat exchanger, Appl. Therm. Eng. 181 (2020) 115950.
[27] Z. Wang, B. Sun, J. Wang, L. Hou, Experimental study on the friction coefficient of supercritical carbon dioxide in pipes, Int. J. Greenh. Gas. Control. 25 (2014) 151–161.
[28] H.K. Tam, L.M. Tam, A.J. Ghajar, Effect of inlet geometries and heating on the entrance and fully-developed friction factors in the laminar and transition regions of a horizontal tube, Exp. Therm. Fluid. Sci. 44 (2013) 680–696.
[29] R. Sun, G. Song, D. Zhang, J. Deng, G. Su, F. Kulacki, W. Tian, S. Qiu, Experimental study of single-phase flow and heat transfer in rectangular channels under uniform and non-uniform heating, Exp. Therm. Fluid. Sci. 114 (2020) 110055.
[30] R. Karwa, S. Solanki, J. Saini, Heat transfer coefficient and friction factor correlations for the transitional flow regime in rib-roughened rectangular ducts, Int. J. Heat. Mass. Transf. 42 (9) (1999) 1597–1615.
[31] M. Varnaseri, S. Peyghambarzadeh, The effect of polyacrylamide drag reducing agent on friction factor and heat transfer coefficient in laminar, transition and turbulent flow regimes in circular pipes with different diameters, Int. J. Heat. Mass. Transf. 154 (2020) 119815.
[32] C. Wang, P. Gao, S. Tan, Z. Wang, C. Xu, Experimental study of friction and heat transfer characteristics in narrow rectangular channel, Nucl. Eng. Des. 250 (2012) 646–655.
[33] A. Bejan, L. Rocha, S. Lorente, Thermodynamic optimization of geometry: T-and Y-shaped constructs of fluid streams, Int. J. Therm. Sci. 39 (9-11) (2000) 949–960.
[34] C.D. Murray, The physiological principle of minimum work applied to the angle of branching of arteries, J. General. Physiol. 9 (6) (1926) 835.
[35] D. Stephenson, A. Patronis, D.M. Holland, D.A. Lockerby, Generalizing Murray's law: an optimization principle for fluidic networks of arbitrary shape and scale, J. Appl. Phys. 118 (17) (2015).